

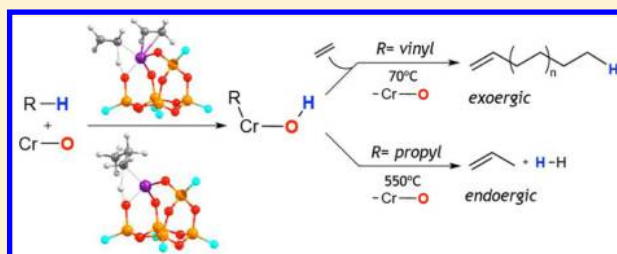
Heterolytic Activation of C–H Bonds on Cr^{III}–O Surface Sites Is a Key Step in Catalytic Polymerization of Ethylene and Dehydrogenation of Propane

Matthew P. Conley,[†] Murielle F. Delley,[†] Francisco Núñez-Zarur,[†] Aleix Comas-Vives, and Christophe Copéret^{*}

Department of Chemistry and Applied Biosciences, ETH Zürich, Vladimir-Prelog-Weg 1–5, CH-8093 Zürich, Switzerland

Supporting Information

ABSTRACT: We describe the reactivity of well-defined chromium silicates toward ethylene and propane. The initial motivation for this study was to obtain a molecular understanding of the Phillips polymerization catalyst. The Phillips catalyst contains reduced chromium sites on silica and catalyzes the polymerization of ethylene without activators or a preformed Cr–C bond. Cr^{II} sites are commonly proposed active sites in this catalyst. We synthesized and characterized well-defined chromium(II) silicates and found that these materials, slightly contaminated with a minor amount of Cr^{III} sites, have poor polymerization activity and few active sites. In contrast, chromium(III) silicates have 1 order of magnitude higher activity. The chromium(III) silicates initiate polymerization by the activation of a C–H bond of ethylene. Density functional theory analysis of this process showed that the C–H bond activation step is heterolytic and corresponds to a σ -bond metathesis type process. The same well-defined chromium(III) silicate catalyzes the dehydrogenation of propane at elevated temperatures with activities similar to those of a related industrial chromium-based catalyst. This reaction also involves a key heterolytic C–H bond activation step similar to that described for ethylene but with a significantly higher energy barrier. The higher energy barrier is consistent with the higher pK_a of the C–H bond in propane compared to the C–H bond in ethylene. In both cases, the rate-determining step is the heterolytic C–H bond activation.



INTRODUCTION

The activation of small molecules is a common theme in the petrochemical and commodity chemical industries. For example, the synthesis and upgrading of small molecules is central to the Haber–Bosch (N₂/H₂), Fischer–Tropsch (H₂/CO), methane reforming (CH₄/H₂O/CO₂), and methanol-to-olefin processes, to name but a few.¹ In addition to these examples, metathesis, oligomerization, and polymerization of olefins are also crucial industrial examples that in most cases rely on the conversion of small molecules (ethylene, propylene, etc.) to products (olefins, polymers, etc.). Traditionally, the low-molecular-weight olefins for these processes are synthesized by cracking techniques. However, the current abundance of low-molecular-weight alkanes in shale gas has caused a renewed interest in dehydrogenation processes for the production of olefins. The catalysts used industrially for the reactions mentioned above will vary from process to process, although they are exclusively heterogeneous because of the ease of separating the desired product from the reaction mixture and the ability of these catalysts to be easily regenerated.

Supported chromium species have a rich history in the activation of small molecules. Chromium-supported on silica was the first commercialized ethylene polymerization catalyst,² a discovery that predates the discovery of Ziegler–Natta polymerization by roughly 2 years. Related catalysts containing

chromium on oxide supports are efficient dehydrogenation catalysts that can convert propane to propene and H₂,³ an increasingly important process run on industrial scales.⁴ In this Forum Article, we will describe how these two catalytic processes are related by similar heterolytic C–H bond activation steps. We will first summarize the classical and well-defined chromium silicates for ethylene polymerization and then show through combined experimental and computational studies that the well-defined chromium species are also active in the dehydrogenation of propane.

The Phillips Catalyst: A Historical Perspective. In the early 1950s, Banks and Hogan, researchers at Phillips Petroleum, found that chromium oxides supported on silica (CrO_x/SiO₂) catalyzed the polymerization of ethylene in the absence of activators or cocatalysts to form high-density polyethylene (HDPE).^{2,5} The CrO_x/SiO₂ material, typically referred to as the Phillips catalyst, was the first commercialized HDPE catalyst and currently accounts for roughly half of global HDPE production per year.

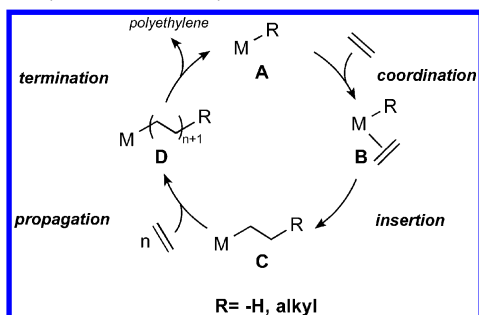
Special Issue: Small Molecule Activation: From Biological Principles to Energy Applications

Received: November 8, 2014



The Phillips catalyst was discovered 2 years prior to Ziegler's discovery of the $\text{TiCl}_4/\text{Et}_2\text{AlCl}$ polymerization catalyst and well before the generally accepted mechanism for the polymerization of olefins catalyzed by homogeneous transition-metal complexes was established.⁶ Extensive studies on homogeneous olefin polymerization catalysts led to the classical insertion mechanism shown in Scheme 1, a mechanism that probably

Scheme 1. Migratory Insertion Mechanism for Transition-Metal-Catalyzed Olefin Polymerization



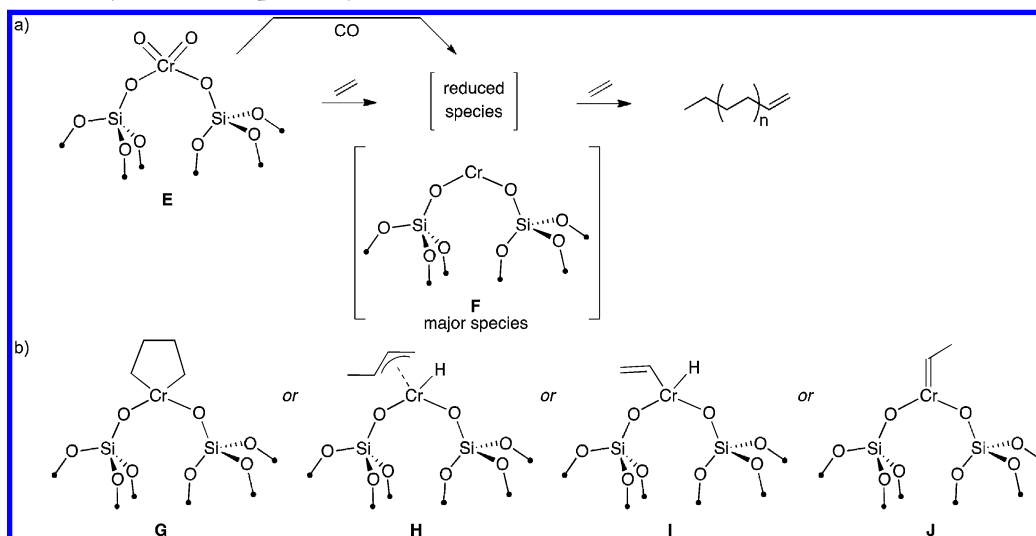
also applies to the heterogeneous Ziegler–Natta catalyst.⁷ An unsaturated metal alkyl **A** is formed by the treatment of a precatalyst with an alkylaluminum cocatalyst⁸ or by activation with a Lewis acid.⁹ **A** coordinates ethylene to form **B** and undergoes migratory insertion to form **C**. Repeating the coordination and insertion of ethylene propagates the polymer chain. Chain transfer or termination releases the polymer and regenerates **A**.¹⁰ This general mechanism applies to a large family of catalysts based on early- and late-transition-metal metals,^{6b,11} which can be either homogeneous and heterogeneous.¹² This mechanism also applies to catalysts that selectively incorporate long-chain branches,¹³ stereoselectively polymerize α -olefins,¹⁴ and control the molecular weight distribution of the polymer.^{11a} The Phillips catalyst polymerizes ethylene without an activator or a preformed Cr–C bond, a unique feature among all known olefin polymerization catalysts.

The Phillips catalyst is prepared by impregnating a silica support with aqueous solutions containing a chromium source, typically CrO_3 or $\text{Cr}(\text{OAc})_3$, followed by a calcination step at high temperatures ($>400\text{ }^\circ\text{C}$). At this stage, the surface species are chromate(VI) esters supported on the silica surface (Scheme 2). At low chromium loadings ($<1\%$ by weight), monomeric Cr^{VI} sites **E** are usually formed on the silica surface,¹⁵ while dimeric and polymeric species can also be obtained at higher loadings. Polymerization of ethylene occurs when **E** is contacted with ethylene to form “reduced” chromium species that are the proposed active sites. Because the Cr^{VI} species must be reduced prior to polymerization initiation, there is a pronounced induction period for polymer formation when using $\text{CrO}_x/\text{SiO}_2$. Alternatively, **E** can be pre-reduced by carbon monoxide (CO) at $300\text{ }^\circ\text{C}$ to produce a catalyst that polymerizes ethylene with a less pronounced induction period.¹⁶

Several leading reviews have shown the difficulty in determining the active site in the Phillips catalyst.¹⁷ Despite these extensive efforts, the active site of the Phillips catalyst is unknown. A major challenge in determining the active site in this catalyst is the presence of only ca. 10% active chromium.¹⁸ Early work by Baker and Carrick showed that ethylene reacts with chromium(VI) silicate to form aldehydes, ketones, and predominately Cr^{II} on the silica surface.¹⁹ In agreement with this report, several spectroscopic studies show that Cr^{II} is the major oxidation state on the surface after treatment with CO.²⁰ In particular, Cr K-edge X-ray absorption spectroscopy (XAS) has been used extensively to study the Phillips catalyst, which showed that isolated species assigned to **F** are the major surface chromium site.²¹

Several initiation species were proposed based on isolated Cr^{II} surface sites (**F**), which are summarized in Scheme 2b. The common theme in each of these proposals is two-electron oxidation of Cr^{II} sites to form Cr^{IV} organometallic intermediates. For example, oxidative coupling of two ethylene molecules would form the chromacyclopentane (**G**), which could insert ethylene by ring expansion.²² Alternatively, **G** can

Scheme 2. (a) Reactivity of the Phillips Catalyst^a



^a(a) The Cr^{VI} -containing silica material (**E**) is reduced by ethylene or by CO to form predominately Cr^{II} on silica (**F**). **F** is proposed to polymerize ethylene. (b) Proposed structures that initiate polymerization: chromacyclopentane species (**G**), chromium allyl hydride (**H**), chromium(IV) vinyl hydride (**I**), or chromium(IV) alkylidene (**J**).

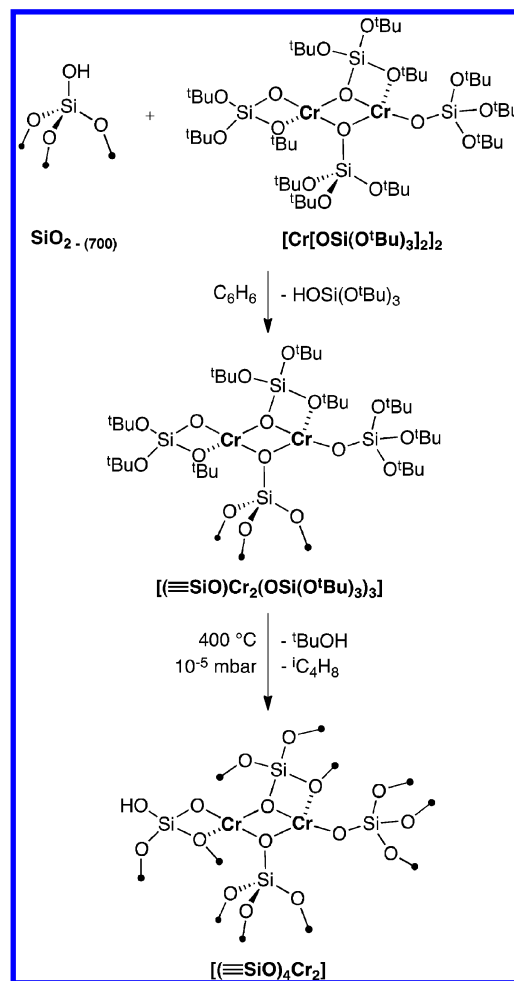
undergo β -hydride elimination to form chromium allyl hydride (H), which can insert ethylene into the Cr–H bond to propagate the polymer.^{5,23} The Cr^{II} sites could also activate a C–H bond of ethylene by oxidative addition to form chromium(IV) vinyl hydride (I)²⁴ or coordinate ethylene and rearrange to chromium(IV) alkydine (J).²⁵ Each of these intermediates could, in principle, polymerize ethylene either by a Cossee–Arman insertion²⁶ (for H and I) or by a Rooney–Green mechanism (for J).²⁷

Although monomeric Cr^{II} surface species are the most commonly proposed active site in the Phillips catalyst, the low quantity of active sites indicates that most of the spectroscopic data are probably related to inactive sites. Indeed, the debate concerning the active sites in the Phillips catalysts is still vigorous, and even the oxidation state of the active sites is controversial. For example, Lunsford et al. showed that chromium(III) salts supported on silica were competent polymerization catalysts.²⁸ Organometallic chromium(III) and chromium(IV) complexes supported on silica are also active in the polymerization of ethylene.^{25a,29} Although Cr^{II} is the predominant oxidation state in a CO-reduced Phillips catalyst, these latter studies indicate that higher oxidation state chromium sites are also competent ethylene polymerization catalyst precursors. The major challenge in determining the active site in the Phillips catalyst, and the formation of the first Cr–C bond, is obtaining a chromium silicate material with a high percentage of active sites, controlled chromium oxidation state, and a coordination environment.

Preparation of Well-Defined Cr/SiO₂ Catalysts. Controlled functionalization of supports with molecular precursors can give well-defined chromium surface species, a general method referred to as surface organometallic chemistry.^{12b,30} Several well-defined chromium surface species have been prepared using this method,^{25a,29a,31} in some cases with the goal to understand the active sites of the Phillips catalyst.³¹ These studies produced catalysts that either already contained a M–C bond or led to chromium(VI) species after calcination, which must undergo the complicated reduction to low-valent chromium discussed above.

Using the thermolytic molecular precursor (TMP) approach developed by Tilley and co-workers,^{31a,b,32} we synthesized silica-supported materials containing “ligandless” chromium silicates with defined oxidation states and nuclearity. This approach involves grafting of a molecular precursor having –OSi(O^tBu)₃ ligands onto silica containing a known concentration of surface silanol groups, followed by thermal treatment of the grafted complex to eliminate the organic residues (isobutene and ^tBuOH). We synthesized a well-defined chromium(II) siloxide [Cr[OSi(O^tBu)₃]₂]₂ and grafted this complex on silica to form [(≡SiO)Cr₂(OSi(O^tBu)₃)₃], as shown in Scheme 3. In TMP, removal of the organic groups is generally accomplished by heating to high temperatures under air, an approach that led to numerous well-defined oxidation catalysts.^{31a,b,32a,33} We desired materials that contained low-oxidation-state chromium. Conducting thermolysis of [(≡SiO)Cr₂(OSi(O^tBu)₃)₃] under vacuum resulted in the release of C₄ organics, which forms [(≡SiO)₄Cr₂] and conserves the oxidation state and nuclearity of the molecular precursor.³⁴ In fact, the X-ray absorption near-edge structure (XANES) of [Cr[OSi(O^tBu)₃]₂]₂, [(≡SiO)Cr₂(OSi(O^tBu)₃)₃] and [(≡SiO)₄Cr₂] contain very similar features, indicating that each contains Cr^{II}, and the coordination environment is similar to that of the molecular complex in [(≡SiO)Cr₂(OSi(O^tBu)₃)₃]

Scheme 3. Reaction of [Cr[OSi(O^tBu)₃]₂]₂ with Silica Dehydroxylated at 700 °C (SiO₂-(700)) To Form [(≡SiO)Cr₂(OSi(O^tBu)₃)₃] and Subsequent Thermal Treatment To Yield [(≡SiO)₄Cr₂]

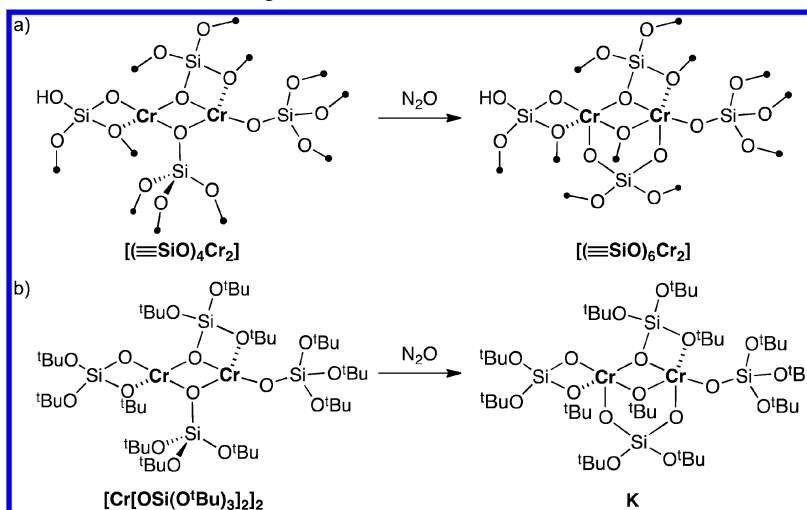


and [(≡SiO)₄Cr₂]. However, the electron paramagnetic resonance (EPR) spectrum of [(≡SiO)₄Cr₂] indicated the presence of traces of Cr^{III} sites (several percent), presumably resulting from the adventitious oxidation Cr^{II} during thermolysis.

[(≡SiO)₄Cr₂], containing mainly Cr^{II} sites, polymerizes ethylene with low activity. Poisoning experiments revealed that only 0.2 equiv of 4-methylpyridine shuts down all polymerization activity, indicating a low amount of active sites in this material. N₂O is a known activator of a CO-reduced Phillips catalyst,^{31d} which prompted us to investigate the activation of [(≡SiO)₄Cr₂] with N₂O. This treatment resulted in a 1 order of magnitude increase in the initial polymerization rate compared to [(≡SiO)₄Cr₂], and a dramatic increase in the quantity of active sites (65% active sites according to quantitative poisoning experiments with 4-methylpyridine). The resulting polyethylene had a large dispersity $\bar{D} = M_w/M_n = 9.4$ (with $M_n = 5500 \text{ g mol}^{-1}$ and $M_w = 52000 \text{ g mol}^{-1}$), which is typical for polymers produced with the Phillips catalyst.

In order to determine the structure of this active catalyst we treated the molecular [Cr[OSi(O^tBu)₃]₂]₂ complex with N₂O, which resulted in isolation of the chromium(III) dimer K shown in Scheme 4. We determined the XAS signature of K [XANES and extended X-ray absorption fine structure

Scheme 4. (a) Reaction of $[(\equiv\text{SiO})_4\text{Cr}_2]$ with N_2O Giving the Chromium(III) Dinuclear Species $[(\equiv\text{SiO})_6\text{Cr}_2]$ and (b) Reaction of $[\text{Cr}[\text{OSi}(\text{O}^t\text{Bu})_3]_2]_2$ with N_2O Giving **K**



(EXAFS)] and $[(\equiv\text{SiO})_4\text{Cr}_2]$ treated with N_2O and found remarkably similar spectral signatures. This result indicates that $[(\equiv\text{SiO})_4\text{Cr}_2]$ reacts with N_2O to form the chromium(III) material $[(\equiv\text{SiO})_6\text{Cr}_2]$ shown in Scheme 4 and established that Cr^{III} sites are active, while Cr^{II} sites display low, if any, polymerization activity.

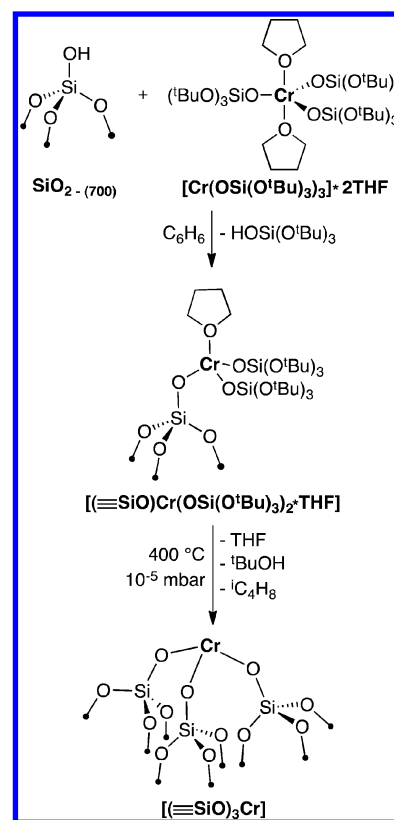
The higher activity of dinuclear chromium(III) silicates than chromium(II) materials is consistent with numerous examples in homogeneous chemistry.³⁵ However, most studies of the Phillips catalyst suggest that monomeric chromium sites are active.^{17b,21} Using the TMP strategy, we synthesized the mononuclear chromium(III) surface species $[(\equiv\text{SiO})_3\text{Cr}]$ from thermolysis of $[(\equiv\text{SiO})\text{Cr}[\text{OSi}(\text{O}^t\text{Bu})_3]_2\cdot\text{THF}]$, as shown in Scheme 5. The similar XANES of $\text{Cr}[\text{OSi}(\text{O}^t\text{Bu})_3]_3\cdot 2\text{THF}$, $[(\equiv\text{SiO})\text{Cr}[\text{OSi}(\text{O}^t\text{Bu})_3]_2\cdot\text{THF}]$, and $[(\equiv\text{SiO})_3\text{Cr}]$ indicates that the Cr^{III} oxidation state is conserved during the grafting and thermolysis steps.³⁶

$[(\equiv\text{SiO})_3\text{Cr}]$ polymerized ethylene to form linear polyethylene with rates and dispersities that are similar to those obtained for the $[(\equiv\text{SiO})_6\text{Cr}_2]$ -catalyzed polymerization of ethylene. Adsorption of CO on $[(\equiv\text{SiO})_3\text{Cr}]$ gives two ν_{CO} stretches in the IR spectrum at 2202 and 2188 cm^{-1} , which are blue-shifted with respect to free CO. According to labeling studies, these two ν_{CO} bands correspond to two different chromium surface sites and not to symmetric and antisymmetric vibrations. Consistent with the presence of different chromium sites in $[(\equiv\text{SiO})_3\text{Cr}]$, roughly 60% of the Cr^{III} surface sites in $[(\equiv\text{SiO})_3\text{Cr}]$ are active in polymerization.

We turned to *ab initio* calculations in order to understand the structure of these different sites. We constructed the two cluster models shown in Figure 1. The first model **1a** contains three Si–O groups coordinated to a Cr^{III} ion, while the second model **1b** incorporates an additional siloxane bridge coordinated to the metal center. The clusters contain six- and eight-membered siloxane rings that are typically observed in bulk silica.³⁷ We completed the silicon environments of both clusters with fluorine, a common approach when using cluster models for silica.^{22b,38}

For all of the calculated stationary points discussed below, we found that the high-spin state ($S = 3/2$) is always more stable than the low-spin one ($S = 1/2$). We calibrated these models by studying the IR frequency of CO coordinated to chromium in

Scheme 5. Preparation of $[(\equiv\text{SiO})_3\text{Cr}]$ by Grafting $\text{Cr}[\text{OSi}(\text{O}^t\text{Bu})_3]_3\cdot 2\text{THF}$ onto $\text{SiO}_2-(700)$ and Subsequent Thermal Treatment



1a and **1b**. The binding of up to three molecules of CO on **1a** is exoergic ($\Delta G = -10.1\text{ kcal mol}^{-1}$). The corresponding $\nu_{\text{CO}}^{\text{symm}}$ and $\nu_{\text{CO}}^{\text{asymm}}$ in **1a-3CO** are blue-shifted by +53 and +46/+50 cm^{-1} with respect to free CO. In contrast, **1b** only binds two molecules of CO ($\Delta G = -8.7\text{ kcal mol}^{-1}$), and the calculated CO vibrations are shifted by +58 and +55 cm^{-1} for the symmetric and antisymmetric modes. Overall, combined experimental [+45 cm^{-1} (major) and +59 cm^{-1} (minor)] and computed frequencies are consistent with the presence of a tricoordinate chromium(III) species as a major surface species,

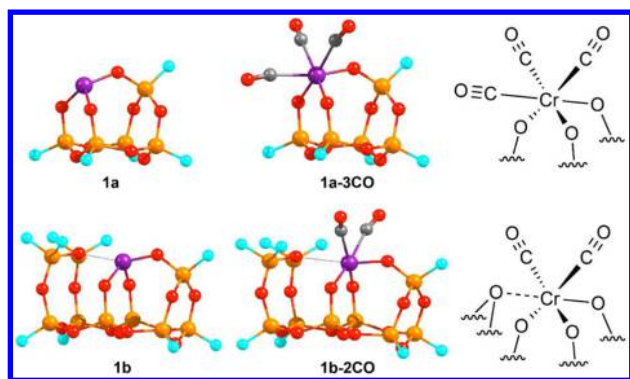


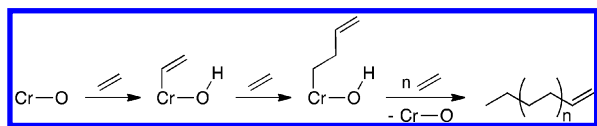
Figure 1. Cluster models constructed to represent Cr^{III} sites in silica and the corresponding CO adducts.

along with a minor species having the Cr^{III} ion coordinated to an additional siloxane bridge. Consistent with these blue-shifted CO signatures, the chromium centers in both **1a** and **1b** carry a partial charge of 1.5+ from natural bond order analysis.

We also modeled the chromium sites using cluster models terminated with –OH groups, resulting in the cluster models **1a'** and **1b'** (Figure S1 in the Supporting Information, SI). The CO binding free energies for the carbonyl adducts in the –OH-terminated clusters are –5.4 and –4.6 kcal mol^{–1} for **1a'** and **1b'**, respectively. The CO stretching bands are blue-shifted with respect to free CO by +42 and +37 cm^{–1} for the symmetric stretching mode and by +39/+36 and +34 cm^{–1} for the antisymmetric stretching mode for **1a'** and **1b'**, respectively. These values are consistent with the experimental data.

Activation and Polymerization Mechanisms. Both [(≡SiO)₆Cr₂] and [(≡SiO)₃Cr] still lack a Cr–C bond necessary to propagate polymerization. We proposed that ethylene reacts with a Cr^{III}–O bond by a heterolytic C–H bond activation mechanism to form chromium vinyl and Si–(μ-OH)–Cr species based on combined experimental and computational studies (Scheme 6).

Scheme 6. Proposed Mechanism of Ethylene Polymerization Involving a Heterolytic Splitting of a C–H Bond across a Cr–O Bond as the Initiation Step



We showed that both [(≡SiO)₆Cr₂] and [(≡SiO)₃Cr] polymerize ethylene without an induction period. In addition, poisoning studies with 4-methylpyridine revealed that most surface sites (ca. 65%) can initiate polymerization. The quantity of the active sites in these materials is significantly higher than that in the Phillips catalysts (<10%) and indicates that the active site can be detected by spectroscopic methods. The XANES of [(≡SiO)₆Cr₂] or [(≡SiO)₃Cr] after exposure to ethylene contains a near-identical edge position relative to pristine [(≡SiO)₆Cr₂] or [(≡SiO)₃Cr], indicating that the Cr^{III} oxidation state is maintained. The polymer produced by either [(≡SiO)₆Cr₂] or [(≡SiO)₃Cr] contains both olefinic and alkyl end groups according to NMR analysis.

We previously proposed that IR spectroscopy could be used to observe the formation of Si–(μ-OH)–Cr. The IR spectrum

of [(≡SiO)₆Cr₂] and [(≡SiO)₃Cr] contacted with ethylene contained strong C–H bands associated with polyethylene, a red-shifted SiOH band interacting with the polymer chain,³⁹ and signals near 3600 cm^{–1} previously assigned to the Si–(μ-OH)–Cr species.^{31c,36} The assignment of Si–(μ-OH)–Cr was based on similar IR signatures of related species in zeolitic materials.⁴⁰ However, the IR spectrum of polyethylene contains combination bands from C–H vibrations at the exact same frequency as that of the Si–(μ-OH)–Cr species.⁴¹ This result indicates that the IR spectra of [(≡SiO)₆Cr₂] and [(≡SiO)₃Cr] after contact with ethylene are dominated by these combination bands, making the unequivocal observation of Si–(μ-OH)–Cr species impossible even with deuterium-labeling experiments.

Using the cluster model of the isolated Cr^{III} site **1a**, we also investigated their reactivity toward ethylene. Calculations of the Gibbs free energies were carried out using standard conditions (25 °C and 1 atm). One or two molecules of ethylene can coordinate to **1a** with favorable energies (see Figure 2). When

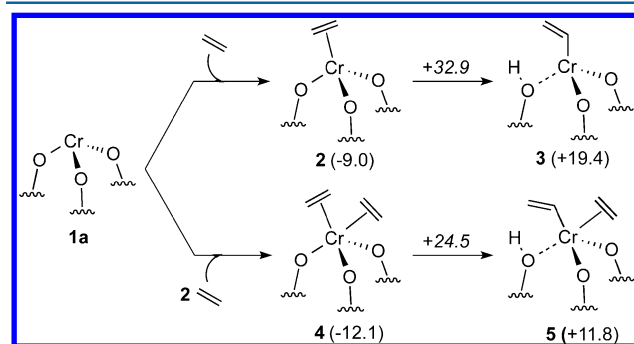


Figure 2. Activation of a C–H bond in ethylene by **1a**. The numbers in parentheses are the Gibbs free energies of the corresponding intermediates, and those on the arrows are the Gibbs free energies of the transition states, normalized with respect to **1a** + ethylene. All energies are given in kcal mol^{–1}.

one molecule of ethylene is coordinated to **1a** to form **2**, C–H bond activation occurs with an intrinsic barrier of 41.9 kcal mol^{–1}. The transition state has the typical structural features associated with σ -bond metathesis,⁴² with a wide O–H–C_{ethylene} angle of about 144° and a C–H distance equal to 1.53 Å, consistent with the heterolytic splitting of a C–H bond in the reaction of **2** to **3**. Coordinating two molecules of ethylene to **1a** forms **4**. In this case, the activation of a C–H bond of ethylene has a lower barrier of 36.6 kcal mol^{–1}. The transition state for the C–H bond activation from **4** is qualitatively similar to that found for **2** with a wide O–H–C_{ethylene} angle of 148° and a C–H distance equal to 1.48 Å, although in this case a second ethylene ligand is coordinated to the chromium center at 2.53 Å.

Exchanging the F-termination in **1a** by –OH groups does not noticeably change the energetics of ethylene C–H bond activation (Figure S3 in the SI).

We also investigated the reactivity of **1b** toward ethylene. The presence of an additional siloxane bridge prevents the coordination of two ethylene molecules and yields a much higher C–H bond activation energy barrier (48.4 kcal mol^{–1}) than that found for **1a**. This result suggests that sites coordinating additional siloxane bridges are inactive in polymerization, which is consistent with the presence of 60% of active sites in [(≡SiO)₃Cr].

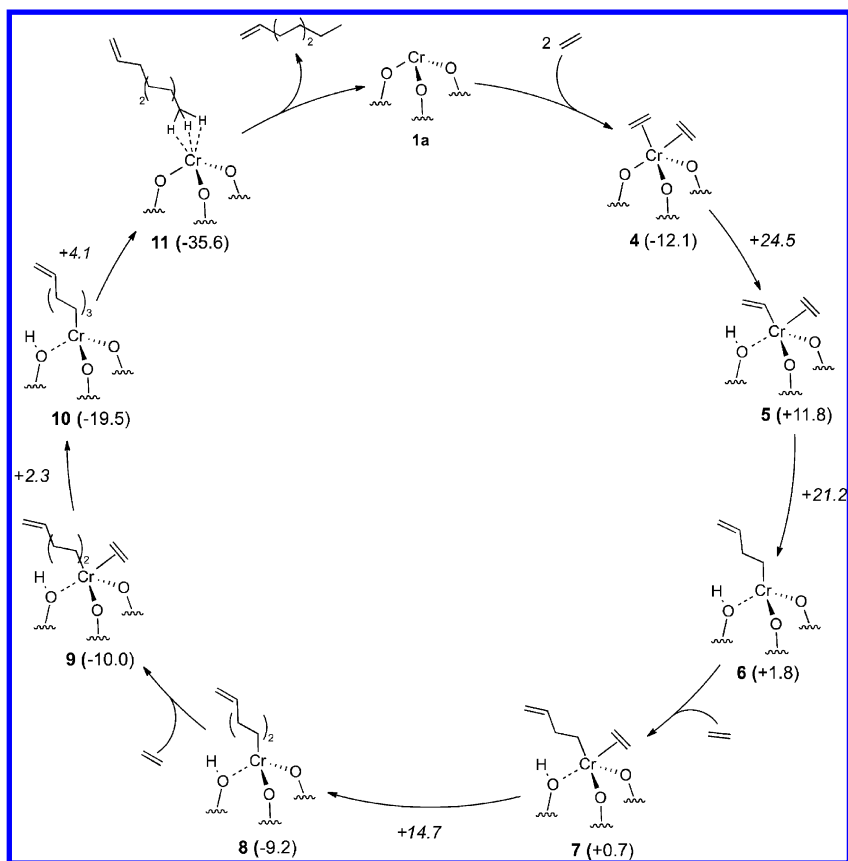


Figure 3. Ethylene polymerization mechanism by **1a**. The numbers in parentheses are the Gibbs free energies of the corresponding intermediate, and those on the arrows are the Gibbs free energies of the transition states, normalized with respect to **1a** + ethylene. All energies are given in kcal mol⁻¹.

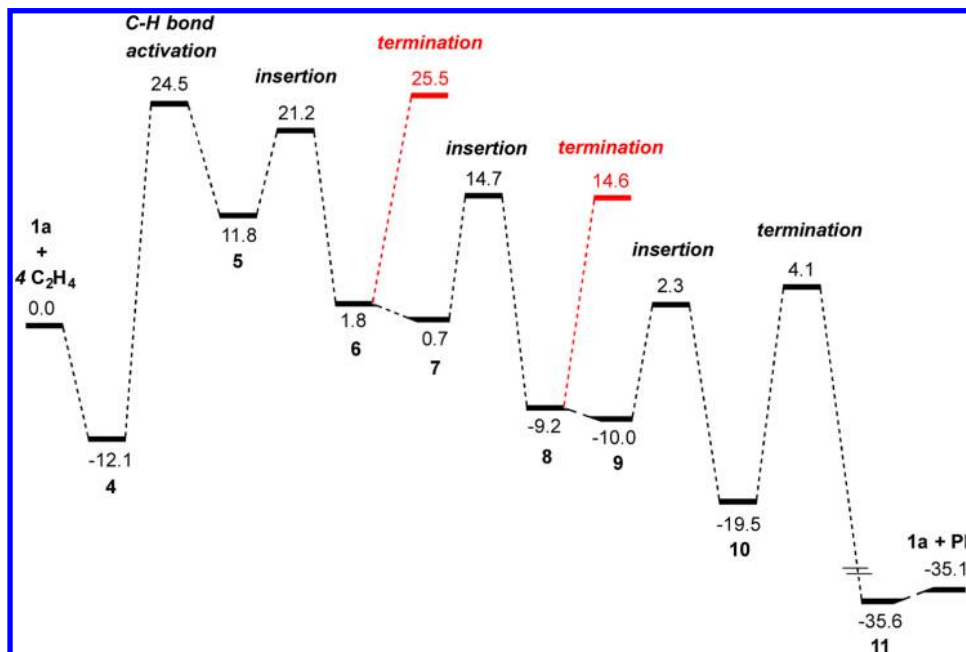


Figure 4. Free-energy profile for the ethylene polymerization reaction by **1a**. All energies are given in kcal mol⁻¹.

We also investigated the species classically proposed in the Phillips catalyst shown in Scheme 2 using the tricoordinate chromium(III) model **1a**. Each surface species in Scheme 2 requires two-electron oxidation at the chromium center, either oxidative coupling or oxidative C–H activation, which would lead to chromium(V) intermediates using **1a**. Neither

chromium vinyl hydride nor chromacycle could be located as stable minima. Optimization of the chromium vinyl hydride species from oxidative C–H activation gives the starting chromium ethylene adduct (**2** in Figure 2). Attempts to optimize the chromacyclic structure of chromium(V) by the coupling of two ethylene molecules led to a chromium alkyl

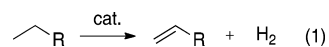
species, where the terminal CH₂ group is about 2.7 Å away from the chromium center, indicating that there is no bond between chromium and that terminal carbon atom (Figure S4 in the SI). This intermediate is 29 kcal mol⁻¹ less stable than separated reactants and therefore unlikely. The difficulty of finding stable chromium(V) species is not too surprising considering the positive redox potential for the reaction Cr⁵⁺ → Cr³⁺ (0.84 V vs NHE).⁴³ Therefore, neither chromium vinyl hydride nor chromacyclic species are likely intermediates in the polymerization of ethylene when chromium(III) species initiate polymerization. These results are also in agreement with the conservation of the 3+ oxidation state during polymerization, as observed by XANES.

Figure 3 shows the proposed catalytic cycle for the formation of an ethylene oligomer catalyzed by **1a**. Two molecules of ethylene coordinate to **1a** to form **4**, one of which undergoes C–H bond activation to form **5**. Species **5** contains a Cr–C bond and a coordinated ethylene that can undergo migratory insertion. After this first insertion, the formation of chromium butenyl (**6**) is only 1.8 kcal mol⁻¹ above the initial reactants. Coordination of an ethylene molecule to **6** forms the π-coordinated species **7**, which is almost thermoneutral with respect to **1a** (+0.7 kcal mol⁻¹). All successive ethylene insertions are exoergic by about 10 kcal mol⁻¹ per inserted ethylene unit, and the intrinsic energy barriers for insertion of ethylene into chromium alkyl are low, ranging from 9.4 to 14.0 kcal mol⁻¹. These energies are typical of M–R-catalyzed olefin insertion.⁴⁴ The most favorable pathway for chain termination corresponds to the proton transfer of Cr–(μ-OH)–Si to chromium alkyl, which is the microreverse of the initial C–H bond activation step on Cr–O sites. Other termination pathways such as direct chain transfer to monomer and β-hydride transfer have less unstable intermediates and/or higher energy barriers than proton transfer.

Figure 4 shows the free-energy profile associated with initiation, polymer growth, and termination involving three ethylene insertions. The C–H bond activation of ethylene is the rate-determining step. The driving force for this reaction is the highly exoergic ethylene insertion reaction (ΔG ≈ -10 kcal mol⁻¹) coupled with low barriers (ΔG[‡] ≈ 9–14 kcal mol⁻¹ for each insertion). Proton transfer to terminate the polymer chains at each chromium alkyl intermediate (red profile in Figure 4) is associated with a higher transition state than insertion (ΔΔG[‡] = 12 kcal mol⁻¹), consistent with polymer growth over termination.

RESULTS AND DISCUSSION

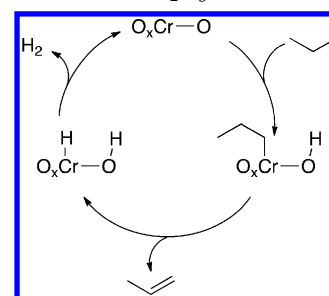
Propane Dehydrogenation Catalyzed by Well-Defined Chromium(III) Silicates. The dehydrogenation of alkanes to alkenes and H₂ (eq 1) is an increasingly important industrial process because of the current abundance of low-molecular-weight alkanes in shale gas.⁴⁵ Not surprisingly, this reaction is highly endoergic and requires high reaction temperatures. In industry, the catalysts are based on either supported PtSn or Cr/Al₂O₃.⁴



Two approaches are generally used to overcome the thermodynamic demands of this reaction, which depend on whether the catalyst is homogeneous or heterogeneous. Brookhart and Goldman have shown that homogeneous (PCP)Ir complexes dehydrogenate alkanes at moderate temperatures in the presence of olefin scavengers, either

added to the reaction mixture or generated in situ.^{46,47} The heterogeneous Cr^{III}/Al₂O₃ dehydrogenation catalyst operates at high temperatures to overcome the thermodynamic limitations of the reaction. Cr^{III}/Al₂O₃ probably activates the C–H bond in propane by a heterolytic mechanism on a Cr–O site, forming chromium alkyl species, as shown in Scheme 7, which

Scheme 7. Proposed Mechanism for Propane Dehydrogenation on Cr^{III}/Al₂O₃



is supported by labeling and *operando* studies of the catalyst.⁴⁸ Chromium alkyl then undergoes β-hydride elimination to release the olefin. The high operating temperatures (>400 °C) allow for the direct liberation of H₂, either by recombination of a Cr–H and a surface O–H to reform isolated Cr^{III} sites or by σ-bond metathesis to regenerate chromium alkyl.^{4,48a} The C–H bond activation step proposed in dehydrogenation parallels the initiation step in ethylene polymerization on well-defined chromium silicates. This led us to investigate the propane dehydrogenation chemistry of [(≡SiO)₃Cr].

The reaction of [(≡SiO)₃Cr] with propane in a continuous-flow reactor (10 mL min⁻¹, 20% in argon, 1.5 bar) forms propene with 72% selectivity. Methane (14%), ethane (2%), and ethylene (11%) are the other products detected (Figures S5–S7 in the SI). Propene is produced with an initial turnover frequency (TOF) of 10.3 h⁻¹ at 550 °C and steadily decreases over 2 h to a TOF of 2.8 h⁻¹. The initial rate and steady decay of activity over time are also typical of classical Cr^{III}/Al₂O₃ catalysts.⁴ The activity of [(≡SiO)₃Cr] in propane dehydrogenation is stable for 20 h after this initial rate decrease, corresponding to a turnover number of 46. All activities and output ratios can be viewed as an upper limit for the equilibrium conversion, where coking is not accounted for (a thermodynamic maximum of 65% of propene is formed at 550 °C in propane dehydrogenation).

Propane Dehydrogenation Pathways. Propane dehydrogenation and associated byproduct formation were also investigated by density functional theory (DFT) calculations using **1a** as a model for the active sites. The free energies were calculated using the experimental conditions 550 °C and 1 atm. The most favorable dehydrogenation pathway catalyzed by **1a** is shown in Figure 5. The formation of a chromium propane η³-H₃H₂H adduct **12** is highly endoergic,⁴⁹ with Cr–H distances between 2.44 and 2.55 Å and a Cr–C distance of 2.63 Å. The heterolytic activation of a C–H bond yields chromium(III) propyl intermediate **13**, an endoergic step of about 17 kcal mol⁻¹, associated with a rather high activation barrier of 57.0 kcal mol⁻¹ with respect to the initial reactants (**1a** + propane). The transition state associated with the C–H bond activation step is again typical for a σ-bond metathesis step with a wide O–H–C_{propane} angle of 150° and a C–H distance equal to 1.58 Å.⁴²

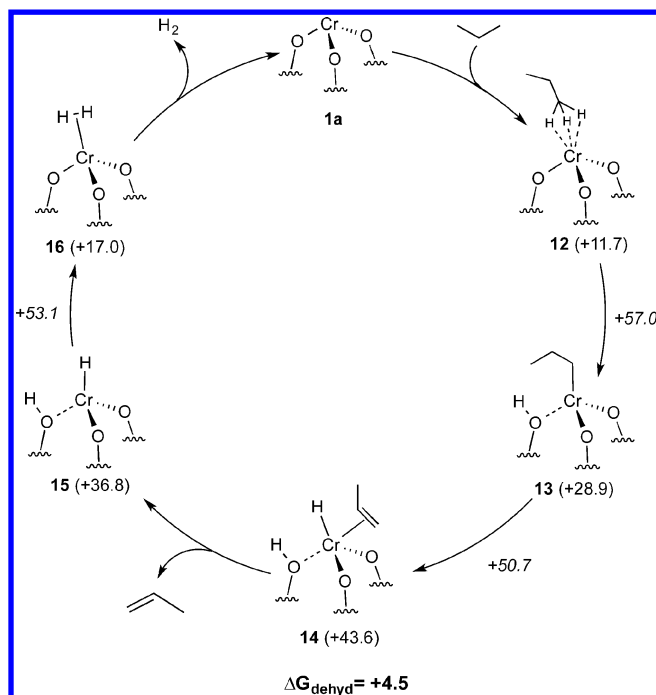


Figure 5. Dehydrogenation of propane catalyzed by **1a**. The numbers in parentheses are the Gibbs free energies of the corresponding intermediates, and those on the arrows are the Gibbs free energies of the transition states, normalized with respect to **1a** + propane. All energies are given in kcal mol⁻¹.

From the chromium(III) propyl intermediate, three pathways for dehydrogenation were investigated. The chromium propyl species **13** can undergo β -H elimination to form the chromium propene hydride surface species **14** (Figure 5). This step is characterized by a late transition state⁵⁰ containing a C–C distance of 1.38 Å, which is very close to that calculated for free propene (1.33 Å). Although **14** is 14.7 kcal mol⁻¹ less stable than **13**, the energy of the transition state from **13** to **14** (+50.7 kcal mol⁻¹) is lower than the energy of the transition

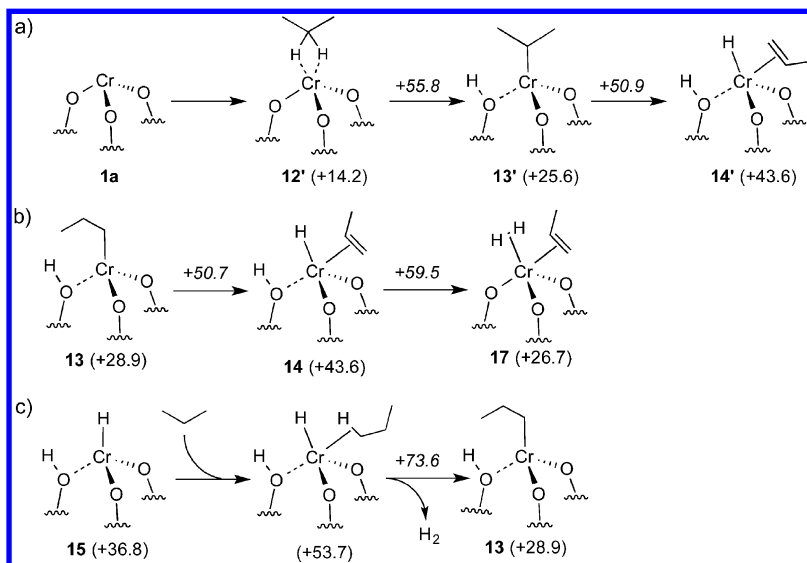
state from **13** to **12** (+57.0 kcal mol⁻¹), indicating that the reaction can proceed via **14**. The subsequent release of propene forms the chromium hydride species **15**. This step is exergonic by 6.8 kcal mol⁻¹. We could not locate the transition state associated with propene loss. The formation of H₂ and completion of the catalytic cycle take place by proton transfer from **15** to form a dihydrogen adduct, Cr(H₂) (**16**), a highly exergonic process by almost 20 kcal mol⁻¹. The transition state is 53.1 kcal mol⁻¹ above that of the initial reactants and displays the typical geometry for proton transfer by a σ -bond metathesis transition state with a wide O–H–H angle (137°) and a H–H distance equal to 1.15 Å.

Alternative pathways were also calculated (Scheme 8). Propane could undergo C–H bond activation at the methylene fragment, leading to **13'**. This C–H bond activation is associated with a slightly lower energy transition state (+55.8 kcal mol⁻¹) than the activation of the primary carbon, leading to **13** (57.0 kcal mol⁻¹). The subsequent β -H transfer from **13'** has an energy profile similar to that of **13**, showing that the rate of formation of propene by either pathway will be only marginally different (Scheme 8a). Other possible pathways that do not involve stepwise β -H transfer, olefin decooordination, and H₂ release are energetically much less favored (Figure S8 in the SI). For example, coupling of the hydrogen atoms in **14** prior to propene release forms the Cr(H₂)(olefin) species **17** and is associated with a high energy barrier (Scheme 8b). Another possibility would be the reaction of a propane molecule with **15** to re-form **13** by a σ -bond metathesis transition state (Scheme 8c). However, each process is associated with very high transition-state energies.

These results show that dehydrogenation occurs by β -H transfer, followed by decooordination of propene, recombination of Si-(μ -OH)-Cr and Cr–H, and release of H₂. The overall thermodynamics for dehydrogenation of propane is calculated to be +4.5 kcal mol⁻¹ at 550 °C, and the rate-determining step is the first C–H bond activation of propane.

Byproduct Formation Pathways. The formation of methane, ethane, and ethylene indicates that cracking processes also occur under experimental conditions. Cracking is

Scheme 8. Alternative Pathways for Dehydrogenation of Propane by (a) Dehydrogenation Pathway through the C–H Bond Activation of the Methylene of Propane, (b) Direct Coupling of the Hydrogen Atoms in **14**, and (c) Regeneration of **13** by σ -Bond Metathesis



associated with similar elementary steps described for dehydrogenation (Figures 6 and 7 and Scheme 9), with the

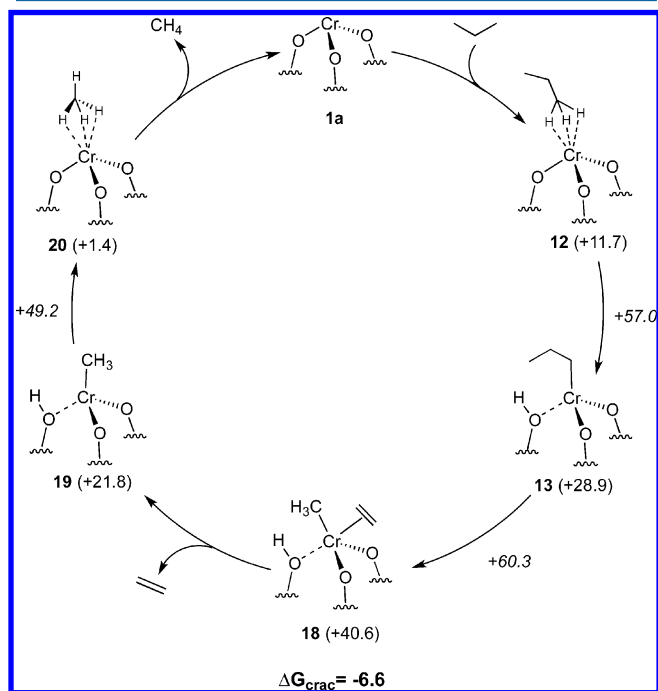


Figure 6. Byproduct formation for the reaction of propane with **1a**. The numbers in parentheses are the Gibbs free energies of the corresponding intermediate, and those on the arrows are the Gibbs free energies of the transition states, normalized with respect to **1a** + propane. All energies are given in kcal mol⁻¹.

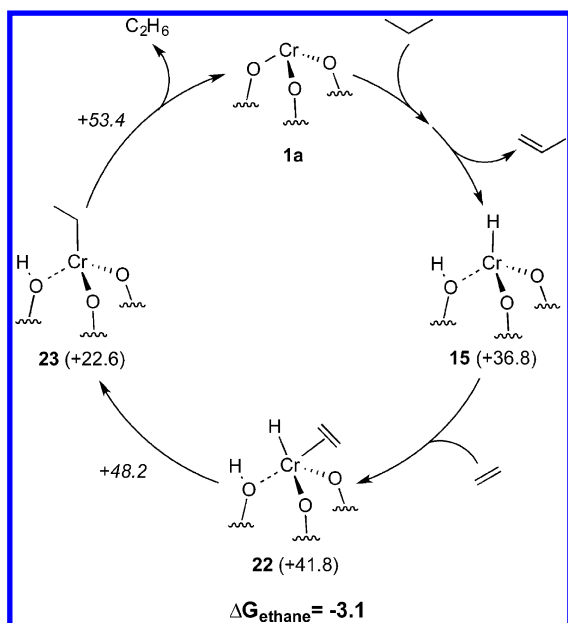
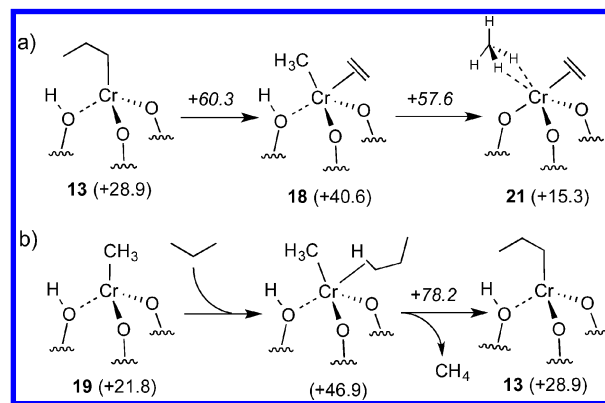


Figure 7. Hydrogenation of ethylene by **1a** to form ethane. The numbers in parentheses are the Gibbs free energies of the corresponding intermediate, and those on the arrows are the Gibbs free energies of the transition states, normalized with respect to **1a** + propane. All energies are given in kcal mol⁻¹.

only difference being cleavage of a C–C bond (β -alkyl transfer) in place of a C–H bond (β -H transfer). The catalytic cycle starts with **12** and the successive heterolytic activation of a C–

Scheme 9. Alternative Pathways for the Cracking of Propane by (a) β -Methyl Transfer Followed by Proton Transfer (b) Regeneration of **13** via σ -Bond Metathesis



H bond of propane, yielding **13**. From **13**, β -alkyl transfer forms the Cr(ethylene)(CH₃) species **18**, an endergonic process by 11.7 kcal mol⁻¹ associated with a transition state of 60.3 kcal mol⁻¹ above separated reactants. **18** releases ethylene to form **19** through an exergonic process of 18.8 kcal mol⁻¹. Subsequent proton transfer from Si-(μ -OH)-Cr to Cr-CH₃ in **19** forms the methane adduct **20** by a transition state that is 49.2 kcal mol⁻¹ above separated reactants (**1a** and propane). Low barrier release of methane regenerates the initial catalyst (**1a**).

We investigated alternative pathways to crack propane (Scheme 9), all of which are similar to the alternative pathways discussed for dehydrogenation of propane (Figure S9 in the SI). The transfer of a proton from Si-(μ -OH)-Cr to Cr-CH₃ prior to ethylene decooordination (Scheme 9a) or σ -bond metathesis between propane and the Cr-CH₃ species **19** (Scheme 9b) is associated with much higher energies than β -Me transfer.

The catalytic cycle for producing methane and ethylene is thermodynamically favored by -6.6 kcal mol⁻¹. However, β -alkyl transfer presents a slightly higher overall energy barrier than the C–H bond activation step (60.3 vs 57.0 kcal mol⁻¹), suggesting that this step is rate-limiting in cracking. This is in contrast to the dehydrogenation reaction, where the C–H bond activation is rate-limiting.

The formation of ethane can proceed by two pathways, with the most favorable one shown in Figure 7; a more complete set of possibilities can be found in the SI (Figure S10). The coordination of ethylene generated from the cracking of propane to **15** forms the π -coordinated species **22**, which inserts ethylene to form the chromium ethyl complex **23**. As expected, the insertion of ethylene into Cr–H is highly exergonic by 14.2 kcal mol⁻¹. Proton transfer from **23** forms ethane and regenerates **1a**. The associated transition states for ethylene insertion and proton transfer are 48.2 and 53.4 kcal mol⁻¹ above separated reactants. Alternatively, ethane can be formed by the direct reaction of ethylene and **13** (Figure S10 in the SI). However, this pathway is associated with higher energy intermediates and higher energy barriers than those of the hydrogenation sequence.

Activation of CH₄ and H₂. Contacting [(≡SiO)₃Cr] with either H₂ or CH₄ at 150 °C does not result in the detection of reaction intermediates (chromium alkyl or hydride) by IR spectroscopy under the explored conditions. Consistent with this observation, the reaction of H₂ and CH₄ on Cr^{III} sites was

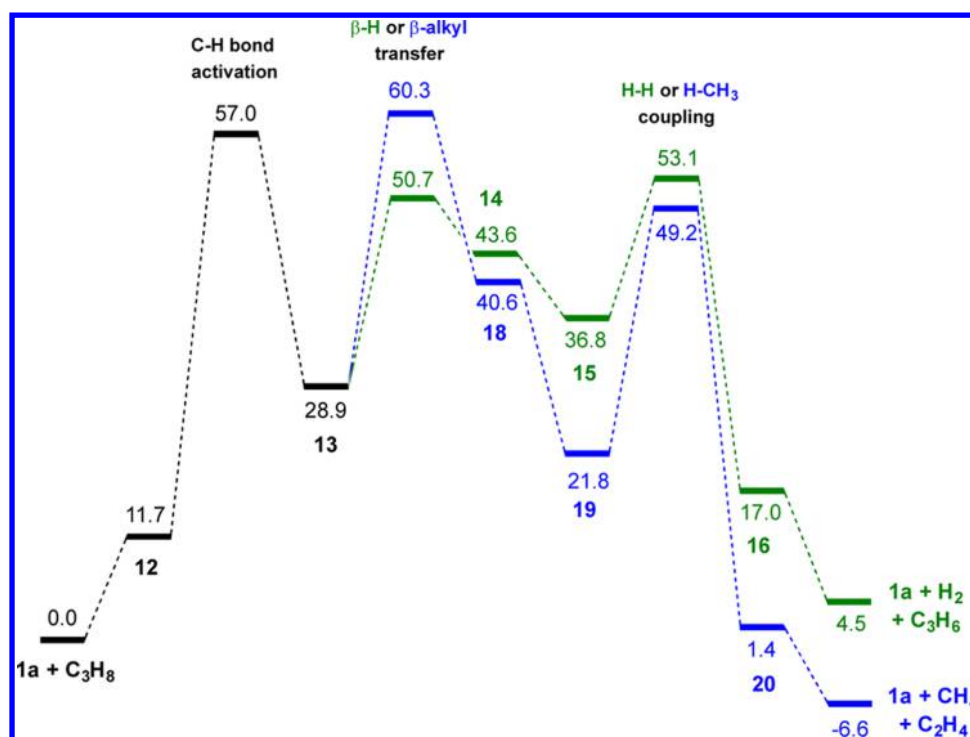


Figure 8. Most favorable free-energy pathways for dehydrogenation (in green) and cracking (in blue) of propane by 1a. All energies are given in kcal mol⁻¹.

calculated to be endergonic by 19.9 and 17.5 kcal mol⁻¹, respectively. The intrinsic barrier to activate H₂ is 32.9 kcal mol⁻¹, while the analogous barrier to activate CH₄ is 40.6 kcal mol⁻¹. However, if a sufficient thermodynamic driving force is present, the activation of H₂ is possible. The hydrogenation of ethylene [(≡SiO)₃Cr] occurs readily at 70 °C with a 1:1 mixture of ethylene and H₂, consistent with the formation of hydride intermediates.

DISCUSSION

The Phillips catalyst is an important industrial catalyst for the production of HDPE. Since the discovery of the Phillips catalyst in 1951, the catalytically active site has been controversial. Counter to several proposals inferring Cr^{II} active sites, we found that well-defined Cr^{III} sites are active while Cr^{II} sites have poor to no activity. This finding is in agreement with several reports in homogeneous catalysis showing that chromium(III) alkyls are active in the polymerization of ethylene.³⁵

The well-defined chromium(III) silicates do not contain a preformed Cr–C bond that is required for olefin polymerization. A mechanism consistent with the NMR of the polymer and XAS data is the heterolytic activation of a C–H bond in ethylene to form a chromium vinyl species that can coordinate and insert ethylene. DFT calculations are in agreement with this proposal and indicate that tricoordinate chromium(III) species are the active sites. Including additional interaction between the Cr^{III} site and an adjacent siloxane bridge in our model leads to significantly higher C–H bond activation barriers, suggesting that these sites are inactive in polymerization. The activation of a C–H bond in ethylene is endoergic and rate-limiting, but coupling with the highly exergonic ethylene insertion steps makes the chromium system an active polymerization catalyst. This proposal parallels what was found for the activation of C–H bonds of methane on γ -alumina,⁵¹ in

which tricoordinate Al^{III}–O sites react with methane through a heterolytic C–H bond activation step. One major difference is that the C–H bond activation step is exoergic on Al^{III}–O sites and endothermic on Cr^{III}–O sites, which leads to observable M–CH₃ surface species on γ -alumina and not on the silica-supported Cr species.

[(≡SiO)₃Cr] also catalyzes the dehydrogenation of propane with 72% selectivity for propene at 550 °C; the byproducts are methane, ethane, and ethylene. DFT analysis shows that the rate-determining step for dehydrogenation is also the C–H bond activation of propane on a Cr–O site (Figure 8). The transition states for β -H- and proton-transfer steps generating propene and H₂ and regenerating 1a are lower in energy than the microreverse of C–H bond activation. The overall reaction is slightly endergonic at 550 °C according to calculation by +4.5 kcal mol⁻¹.

In contrast, the thermodynamics for the formation of methane and ethylene byproducts from propane are actually much more favorable (–6.6 kcal mol⁻¹). However, the key step determining selectivity is the β -X transfer step (X = H, CH₃), which is more favored for dehydrogenation (X = H) than for cracking (X = CH₃) by 9.6 kcal mol⁻¹. These results indicate that C–H bond activation is rate-determining in propane dehydrogenation, while β -methyl transfer is likely rate-limiting for the cracking of propane. However, β -methyl transfer can compete with the initial C–H bond activation of propane because the overall energetic difference between the two transition states is ca. 3 kcal mol⁻¹. This difference is small and indicates that the two processes are competitive, in agreement with the detection of both dehydrogenation and cracking products in the gas phase under experimental conditions.

The activation of an H–X bond (X = H, CH₃, C₂H₃, C₃H₇) is endoergic in all cases explored here. With the calculated transition states, we can now compare the activation step for each substrate. Figure 9 shows the transition states for the

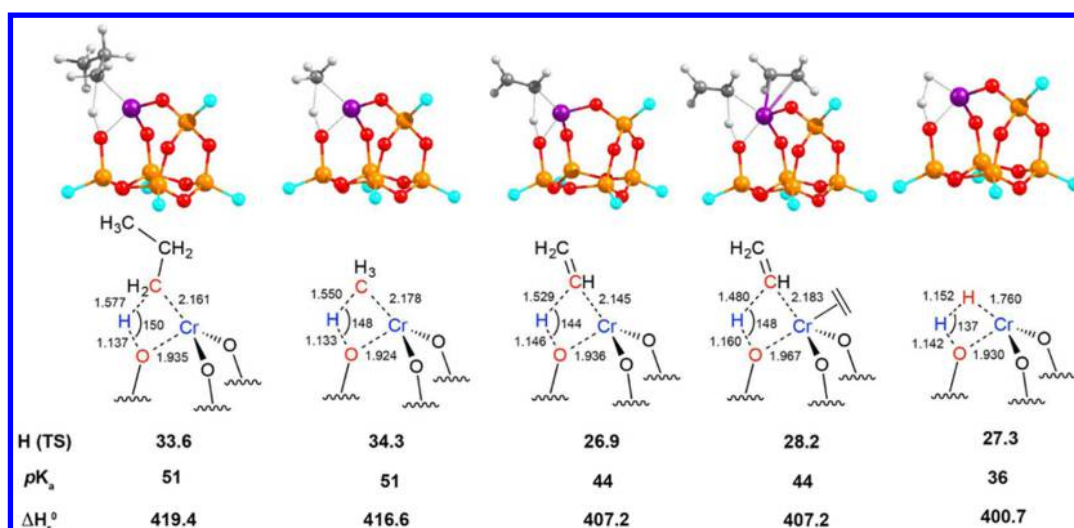


Figure 9. Transition-state structures for the X–H bond activation in C_3H_8 , CH_4 , C_2H_4 , and H_2 . The enthalpic transition-state energy [$H(TS)$] at 298 K and 1 atm (in kcal mol^{-1} , calculated with respect to separated reactants with the BS1 basis set and no dispersion correction) for the activation of the X–H bond, the pK_a value, and the gas-phase acidities (ΔH_r° , in $\text{kcal}\cdot\text{mol}^{-1}$) for all substrates are given below the structures.

activation of C_3H_8 , CH_4 , C_2H_4 , and H_2 and gives their energy compared to separated reactants under standard conditions (25 °C and 1 atm). The barriers of the H–X bond activation step decrease in the order propane \approx methane > ethylene \approx H_2 . The transition-state structures for the activation processes of all of these substrates are remarkably similar. All of the transition-state structures contain wide O–H–X angles ranging from 137° to 150° and a H–X distance ranging between 1.15 and 1.55 Å. The lowest values are for H_2 and ethylene, while the values for saturated hydrocarbons are very similar. In all cases, a formal four-center σ -bond metathesis transition state, consistent with the heterolytic cleavage of the H–X bond, was obtained.^{42,51c,52} Analysis of the partial charges in these transition-state structures indicates that the chromium ion and the activated C–H bond carry partial positive charges (atoms in blue), while the oxygen acceptor of the proton and the “X” group carry a partial negative charge (atoms in red). The easier activation of C_{sp_2} –H over C_{sp_3} –H bonds can be related to the difference of pK_a values and the gas-phase acidities of these substrates (ΔH_r°), which is also consistent with a heterolytic activation process.^{51c,52c} The slightly disfavored H_2 activation on Cr^{III} –O sites in comparison to ethylene is likely due to the shorter H–H versus C–H bond.

CONCLUSION

The initial motivation of this endeavor was to obtain a molecular understanding of the active sites in the Phillips catalyst. Although numerous studies conclude that isolated Cr^{II} sites are active in olefin polymerization, we found that well-defined dinuclear chromium(II) silicates have, at best, poor activity. In contrast, well-defined Cr^{III} sites are active. The heterolytic C–H bond activation of ethylene forms the first Cr–C bond in these well-defined Cr^{III} -containing materials, as well as for the CO-reduced Phillips catalyst. The C–H bond activation step is rate-determining and follows a σ -bond-metathesis-type transition state. The microreverse of the C–H bond activation (chain transfer) has a higher barrier than the insertion of ethylene into a chromium alkyl, which leads to polymer growth.

The chromium(III) silicates also catalyze the dehydrogenation of propane to form propene and H_2 at 550 °C with rates that are similar to the industrial catalysts. Dehydrogenation also occurs by the C–H bond activation of propane on a Cr–O bond. The transition state also has σ -bond metathesis character and structural similarity to that obtained for the C–H bond activation of ethylene. The calculated barrier to heterolytic activation of the C–H bond of propane is much higher than that found for ethylene, consistent with the higher pK_a value for the C–H bond of propane, as expected for a heterolytic C–H bond activation process.

These studies establish that silica-supported Cr^{III} sites can activate C–H bonds of small hydrocarbons by a σ -bond metathesis mechanism. The highly reactive intermediates generated by C–H bond activation lead to subsequent catalytic reactivity in polymerization or dehydrogenation. We expect that the heterolytic C–H bond activation encountered in these studies is general and will lead to new materials capable of activating small molecules by similar or related mechanisms. We are currently exploring this possibility.

EXPERIMENTAL SECTION

General Considerations. All manipulations were performed under an inert gas atmosphere using Schlenk (argon), glovebox (argon), or high-vacuum (10^{-5} mbar) techniques. O_2 and water were removed from all gases (propane, ethylene, methane, and H_2) by passing them through a copper catalyst (R3-11, BASF) and activated 4 Å molecular sieves before use. IR spectra were recorded in transmission mode on a Nicolet 6700 FT-IR spectrophotometer. Catalytic experiments under gas-flow conditions were performed in a flow reactor made of stainless steel SS316 (diameter 1.4 cm) surrounded by an oven connected via a thermocouple reaching into the catalyst mixed with SiC (2.5 g). The synthesis of $[(\equiv SiO)_6Cr_2]$ and $[(\equiv SiO)_3Cr]$ and experimental details for the polymerization of ethylene using these materials were described previously.^{31c,36}

Propane Dehydrogenation Using $[(\equiv SiO)_3Cr]$. $[(\equiv SiO)_3Cr]$ (60 mg, 0.011 mmol of chromium) was mixed with SiC (2.5 g) and placed in a flow reactor. Argon was flowed through the reactor (10 mL min^{-1}), while the reactor was heated to 550 °C. At this temperature, a mixture of propane and argon (10 mL min^{-1} ; 1:4 propane/argon; gas hourly space velocity = 353 h^{-1}) was passed through the reactor, and the output gases were monitored by gas chromatography with a flame ionization detector (FID-GC) for 20 h.

Reactivity of $[(\equiv\text{SiO})_3\text{Cr}]$ toward Propane. A disk of $[(\equiv\text{SiO})_3\text{Cr}]$ (30 mg, 0.006 mmol of chromium) was contacted with propane (150 mbar, 310 equiv per chromium) at room temperature for 30 min, then at 100 °C for 30 min, then at 150 °C for 30 min, then at 300 °C for 30 min, then at 400 °C for 5 h, and then at 500 °C for 14 h. The reaction was monitored by IR transmission; after heating at each temperature, two IR spectra were collected with and without condensation of the gas phase. After the experiment, FID-GC of the gas phase was performed, which apart from propane showed methane (0.02 mmol, 3.2 equiv per chromium), ethane (0.01 mmol, 1.5 equiv per chromium), ethylene (0.01 mmol, 1.2 equiv per chromium), and propylene (0.10 mmol, 15.4 equiv per chromium). The gas phase was then evacuated under high vacuum (10^{-5} mbar) for 1 h, and another IR spectrum was recorded.

Reactivity of $[(\equiv\text{SiO})_3\text{Cr}]$ toward CH_4 Monitored by IR Spectroscopy. A disk of $[(\equiv\text{SiO})_3\text{Cr}]$ (30 mg, 0.006 mmol of chromium) was contacted with methane (150 mbar, 320 equiv per chromium) at room temperature for 1 h, then at 100 °C for 1 h, and then at 150 °C for 1 h and monitored by IR transmission spectrometry after heating at each temperature. The gas phase was evacuated under high vacuum (10^{-5} mbar) for 1 h, and another IR spectrum was recorded.

Reactivity of $[(\equiv\text{SiO})_3\text{Cr}]$ toward H_2 . A disk of $[(\equiv\text{SiO})_3\text{Cr}]$ (30 mg, 0.006 mmol of chromium) was contacted with H_2 (150 mbar, 320 equiv per chromium) at room temperature for 1 h, then at 100 °C for 1 h, and then at 150 °C for 1 h and monitored by IR transmission spectrometry after heating at each temperature. The gas phase was evacuated under high vacuum (10^{-5} mbar) for 1 h, and another IR spectrum was recorded.

Hydrogenation of Ethylene with $[(\equiv\text{SiO})_3\text{Cr}]$ Using H_2 . $[(\equiv\text{SiO})_3\text{Cr}]$ on a Grace Sylopol 948 (40 mg, 0.012 mmol of chromium) was preheated at 70 °C and then contacted with a 1:1 mixture of $\text{H}_2/\text{C}_2\text{H}_4$ (650 mbar, 680 equiv of $\text{H}_2/\text{C}_2\text{H}_4$ mixture per chromium) for 5 h. The gas phase was monitored and analyzed by IR and FID-GC and GC–mass spectrometry. After 4 h, the gas phase contained, apart from ethylene and H_2 , ethane (11 equiv per chromium) and traces of butane (0.085 equiv per chromium) and hexane (0.022 equiv per chromium). After the experiment, the surface was characterized via IR and ^1H and ^{13}C NMR, which evidenced the formation of polyethylene on the surface.

COMPUTATIONAL DETAILS

The theoretical calculations were carried out at the DFT level with the B3LYP hybrid density functional,⁵³ as implemented in the Gaussian 09 suite of programs.⁵⁴ All considered reaction pathways were calculated with the high-spin configuration of the $\text{Cr}^{\text{III}} d^3$ ion ($S = 3/2$) because the doublet is much higher in energy and no spin crossing was detected in the potential energy surface exploration. Geometries were obtained through a combination of basis sets (BS1): the LanL2DZ⁵⁵ effective core potential of Hay and Wadt for chromium and the 6-311G(d,p)⁵⁶ basis set for all other atoms. The nature of all stationary points along the potential energy surfaces was confirmed by computation of the Hessian matrix, obtaining no imaginary frequencies for minima and only one for transition-state structures. Intrinsic reaction coordinate calculations were carried out in the C–H bond activation steps to ensure that the transition states connect properly with the reactants and products. Gas-phase thermal corrections were calculated at standard conditions (25 °C and 1 atm) for the ethylene polymerization reaction and at 550 °C and 1 atm for the propane dehydrogenation reaction, including the formation of byproducts. These calculations allow us to obtain entropic contributions in the reaction pathways. Electronic energies were refined with extended basis sets (BS2): LanL2TZ(f)^{55a,57} for chromium and 6-311++G(d,p)^{56,58} for all other atoms. Additionally, Grimme's D3 dispersion corrections⁵⁹ with Becke and Johnson damping⁶⁰ were added to the final energies.

ASSOCIATED CONTENT

Supporting Information

Listings of selectivity, activity, and conversion data for propane dehydrogenation and further DFT calculations. This material is available free of charge via the Internet at <http://pubs.acs.org>.

AUTHOR INFORMATION

Corresponding Author

*E-mail: ccoperet@ethz.ch. Phone: +41446339394.

Author Contributions

†These authors contributed equally to the work.

Notes

The authors declare no competing financial interest.

ACKNOWLEDGMENTS

M.F.D. thanks ETH Zürich and the Scholarship Fund of the Swiss Chemical Industry for financial support. A.C.-V. acknowledges support from the Swiss National Foundation (Grant PZ00P2_148059).

DEDICATION

Dedicated to Prof. E. Negishi on the occasion of his 80th birthday.

REFERENCES

- (1) (a) Lloyd, L. *Handbook of Industrial Catalysts*; Springer: Berlin, 2011. (b) Bartholomew, C. H. F.; Robert, J. *Fundamentals of Industrial Catalytic Processes*, 2nd ed.; John Wiley & Sons, Inc.: New York, 2006.
- (2) McDaniel, M. P. A Review of the Phillips Supported Chromium Catalyst and Its Commercial Use for Ethylene Polymerization. In *Advances in Catalysis*; Bruce, C. G., Helmut, K., Eds.; Academic Press: New York, 2010; Chapter 3.
- (3) Resasco, D. E. Dehydrogenation–Heterogeneous. In *Encyclopedia of Catalysis*; John Wiley & Sons, Inc.: New York, 2002.
- (4) Sattler, J. J. H. B.; Ruiz-Martinez, J.; Santillan-Jimenez, E.; Weckhuysen, B. M. *Chem. Rev.* **2014**, *114*, 10613–10653.
- (5) McDaniel, M. P. Supported Chromium Catalysts for Ethylene Polymerization. In *Advances in Catalysis*; Eley, H. P. D. D., Paul, B. W., Eds.; Academic Press: New York, 1985.
- (6) (a) Rappé, A. K.; Skiff, W. M.; Casewit, C. J. *Chem. Rev.* **2000**, *100*, 1435–1456. (b) Ittel, S. D.; Johnson, L. K.; Brookhart, M. *Chem. Rev.* **2000**, *100*, 1169–1204.
- (7) Corradini, P.; Guerra, G.; Cavallo, L. *Acc. Chem. Res.* **2004**, *37*, 231–241.
- (8) Kaminsky, W. *J. Chem. Soc., Dalton Trans.* **1998**, 1413–1418.
- (9) Chen, E. Y.-X.; Marks, T. J. *Chem. Rev.* **2000**, *100*, 1391–1434.
- (10) Amin, S. B.; Marks, T. J. *Angew. Chem., Int. Ed.* **2008**, *47*, 2006–2025.
- (11) (a) Coates, G. W.; Hustad, P. D.; Reinartz, S. *Angew. Chem., Int. Ed.* **2002**, *41*, 2236–2257. (b) Nakamura, A.; Anselment, T. M. J.; Claverie, J.; Goodall, B.; Jordan, R. F.; Mecking, S.; Rieger, B.; Sen, A.; van Leeuwen, P. W. N. M.; Nozaki, K. *Acc. Chem. Res.* **2013**, *46*, 1438–1449.
- (12) (a) Marks, T. J. *Acc. Chem. Res.* **1992**, *25*, 57–65. (b) Wegener, S. L.; Marks, T. J.; Stair, P. C. *Acc. Chem. Res.* **2011**, *45*, 206–214. (c) Nicholas, C. P.; Ahn, H.; Marks, T. J. *J. Am. Chem. Soc.* **2003**, *125*, 4325–4331. (d) Jezequel, M.; Dufaud, V.; Ruiz-Garcia, M. J.; Carrillo-Hermosilla, F.; Neugebauer, U.; Nicolai, G. P.; Lefebvre, F.; Bayard, F.; Corker, J.; Fiddy, S.; Evans, J.; Broeyer, J.-P.; Malinge, J.; Basset, J.-M. *J. Am. Chem. Soc.* **2001**, *123*, 3520–3540. (e) Joubert, J.; Delbecq, F.; Sautet, P.; Roux, E. L.; Taoufik, M.; Thieuleux, C.; Blanc, F.; Copéret, C.; Thivolle-Cazat, J.; Basset, J.-M. *J. Am. Chem. Soc.* **2006**, *128*, 9157–9169.
- (13) Braunschweig, H.; Breitling, F. M. *Coord. Chem. Rev.* **2006**, *250*, 2691–2720.

- (14) Coates, G. W. *Chem. Rev.* **2000**, *100*, 1223–1252.
- (15) McDaniel, M. P.; Collins, K. S.; Benham, E. A. *J. Catal.* **2007**, *252*, 281–295.
- (16) Zecchina, A.; Garrone, E.; Ghiotti, G.; Morterra, C.; Borello, E. *J. Phys. Chem.* **1975**, *79*, 966–972.
- (17) (a) Weckhuysen, B. M.; Schoonheydt, R. A. *Catal. Today* **1999**, *51*, 215–221. (b) Groppo, E.; Lamberti, C.; Bordiga, S.; Spoto, G.; Zecchina, A. *Chem. Rev.* **2005**, *105*, 115–184.
- (18) McDaniel, M. P.; Martin, S. J. *J. Phys. Chem.* **1991**, *95*, 3289–3293.
- (19) Baker, L. M.; Carrick, W. L. *J. Org. Chem.* **1968**, *33*, 616–618.
- (20) (a) Weckhuysen, B. M.; Wachs, I. E.; Schoonheydt, R. A. *Chem. Rev.* **1996**, *96*, 3327–3350. (b) Chakrabarti, A.; Wachs, I. E. *Catal. Lett.* **2014**, *144*, 1–10.
- (21) Bordiga, S.; Groppo, E.; Agostini, G.; van Bokhoven, J. A.; Lamberti, C. *Chem. Rev.* **2013**, *113*, 1736–1850.
- (22) (a) Rebenstorf, B.; Larsson, R. *J. Mol. Catal.* **1981**, *11*, 247–256. (b) Espelid, O.; Borve, K. J. *J. Catal.* **2002**, *206*, 331–338. (c) Groppo, E.; Lamberti, C.; Bordiga, S.; Spoto, G.; Zecchina, A. *J. Catal.* **2006**, *240*, 172–181.
- (23) Ruddick, V. J.; Badyal, J. P. S. *J. Phys. Chem. B* **1998**, *102*, 2991–2994.
- (24) Cheng, R.; Liu, Z.; Zhong, L.; He, X.; Qiu, P.; Terano, M.; Eisen, M.; Scott, S.; Liu, B. Phillips Cr/Silica Catalyst for Ethylene Polymerization. In *Polyolefins: 50 years after Ziegler and Natta I*; Kaminsky, W., Ed.; Springer: Berlin, 2013.
- (25) (a) Amor Nait Ajjou, J.; Scott, S. L.; Paquet, V. *J. Am. Chem. Soc.* **1998**, *120*, 415–416. (b) Ghiotti, G.; Garrone, E.; Zecchina, A. *J. Mol. Catal.* **1988**, *46*, 61–77. (c) Rebenstorf, B. *J. Mol. Catal.* **1988**, *45*, 263–274. (d) Liu, B.; Nakatani, H.; Terano, M. *J. Mol. Catal. A: Chem.* **2003**, *201*, 189–197. (e) Amor Nait Ajjou, J.; Scott, S. L. *Organometallics* **1997**, *16*, 86–92. (f) Ghiotti, G.; Garrone, E.; Coluccia, S.; Morterra, C.; Zecchina, A. *J. Chem. Soc., Chem. Commun.* **1979**, 1032–1033.
- (26) (a) Cossee, P. *J. Catal.* **1964**, *3*, 80–88. (b) Arlman, E. J. *J. Catal.* **1964**, *3*, 89–98. (c) Arlman, E. J.; Cossee, P. *J. Catal.* **1964**, *3*, 99–104.
- (27) Ivin, K. J.; Rooney, J. J.; Stewart, C. D.; Green, M. L. H.; Mahtab, R. *J. Chem. Soc., Chem. Commun.* **1978**, 604–606.
- (28) (a) Przhivalskaya, L. K.; Shvets, V. A.; Kazansky, V. B. *J. Catal.* **1975**, *39*, 363–368. (b) Myers, D. L.; Lunsford, J. H. *J. Catal.* **1986**, *99*, 140–148.
- (29) (a) Amor Nait Ajjou, J.; Scott, S. L. *J. Am. Chem. Soc.* **2000**, *122*, 8968–8976. (b) Ikeda, H.; Monoi, T.; Sasaki, Y. *J. Polym. Sci., Part A: Polym. Chem.* **2003**, *41*, 413–419. (c) Monoi, T.; Haruhiko, H. I.; Hiroyuki, O.; Yasuaki, S. *Polym. J.* **2002**, *34*, 461–465. (d) Takashi, M.; Haruhiko, I.; Yasuaki, S.; Yasumichi, M. *Polym. J.* **2003**, *35*, 608–611.
- (30) (a) Copéret, C.; Chabanas, M.; Petroff Saint-Arroman, R.; Basset, J.-M. *Angew. Chem., Int. Ed.* **2003**, *42*, 156–181. (b) Tada, M.; Iwasawa, Y. *Coord. Chem. Rev.* **2007**, *251*, 2702–2716. (c) Thomas, J. M.; Raja, R.; Lewis, D. W. *Angew. Chem., Int. Ed.* **2005**, *44*, 6456–6482.
- (31) (a) Fujidala, K. L.; Tilley, T. D. *J. Catal.* **2003**, *216*, 265–275. (b) Fujidala, K.; Brutchey, R.; Tilley, T. D. Tailored Oxide Materials via Thermolytic Molecular Precursor (TMP) Methods. In *Surface and Interfacial Organometallic Chemistry and Catalysis*; Copéret, C.; Chaudret, B., Eds.; Springer: Berlin, 2005. (c) Conley, M. P.; Delley, M. F.; Siddiqi, G.; Lapadula, G.; Norsic, S.; Monteil, V.; Safonova, O. V.; Coperet, C. *Angew. Chem., Int. Ed.* **2014**, *53*, 1872–1876. (d) Groppo, E.; Damin, A.; Otero Arean, C.; Zecchina, A. *Chem.—Eur. J.* **2011**, *17*, 11110–11114.
- (32) (a) Coles, M. P.; Lugmair, C. G.; Terry, K. W.; Tilley, T. D. *Chem. Mater.* **2000**, *12*, 122–131. (b) Terry, K. W.; Gantzel, P. K.; Tilley, T. D. *Inorg. Chem.* **1993**, *32*, 5402–5404. (c) Terry, K. W.; Lugmair, C. G.; Tilley, T. D. *J. Am. Chem. Soc.* **1997**, *119*, 9745–9756.
- (33) Fujidala, K. L.; Tilley, T. D. *Chem. Mater.* **2001**, *13*, 1817–1827.
- (34) Conley, M.; Copéret, C. *Top. Catal.* **2014**, *57*, 843–851.
- (35) (a) Theopold, K. H. *Eur. J. Inorg. Chem.* **1998**, 1998, 15–24. (b) MacAdams, L. A.; Buffone, G. P.; Incarvito, C. D.; Rheingold, A. L.; Theopold, K. H. *J. Am. Chem. Soc.* **2005**, *127*, 1082–1083. (c) Thomas, B. J.; Noh, S. K.; Schulte, G. K.; Sendlinger, S. C.; Theopold, K. H. *J. Am. Chem. Soc.* **1991**, *113*, 893–902.
- (36) Delley, M. F.; Nunez-Zarur, F.; Conley, M. P.; Comas-Vives, A.; Siddiqi, G.; Norsic, S.; Monteil, V.; Safonova, O. V.; Coperet, C. *Proc. Natl. Acad. Sci. U. S. A.* **2014**, *111*, 11624–11629.
- (37) (a) Stallons, J. M.; Iglesia, E. *Chem. Eng. Sci.* **2001**, *56*, 4205–4216. (b) Zhuravlev, L. T. *Colloid Surf. A* **2000**, *173*, 1–38.
- (38) (a) Espelid, O.; Borve, K. J. *J. Catal.* **2000**, *195*, 125–139. (b) Espelid, O.; Borve, K. J. *Catal. Lett.* **2001**, *75*, 49–54. (c) Espelid, O.; Borve, K. J. *J. Catal.* **2002**, *205*, 177–190. (d) Espelid, O.; Borve, K. J. *J. Catal.* **2002**, *205*, 366–374.
- (39) van der Meer, J.; Bardez-Giboire, I.; Mercier, C.; Revel, B.; Davidson, A.; Denoyel, R. *J. Phys. Chem. C* **2010**, *114*, 3507–3515.
- (40) (a) Dzwigaj, S.; Shishido, T. *J. Phys. Chem. C* **2008**, *112*, 5803–5809. (b) Hadjiivanov, K.; Penkova, A.; Kefirov, R.; Dzwigaj, S.; Che, M. *Microporous Mesoporous Mater.* **2009**, *124*, 59–69. (c) Tielens, F.; Islam, M. M.; Skara, G.; De Proft, F.; Shishido, T.; Dzwigaj, S. *Microporous Mesoporous Mater.* **2012**, *159*, 66–73. (d) Cappus, D.; Xu, C.; Ehrlich, D.; Dillmann, B.; Ventrice, C. A., Jr.; Al Shamery, K.; Kuhlbeck, H.; Freund, H. J. *Chem. Phys.* **1993**, *177*, 533–546.
- (41) We thank a reviewer of this manuscript for directing us to literature data containing the FTIR spectrum of HDPE. The FTIR spectrum of HDPE synthesized in these studies is given in the SI (Figure S2).
- (42) (a) Balcells, D.; Clot, E.; Eisenstein, O. *Chem. Rev.* **2010**, *110*, 749–823. (b) Waterman, R. *Organometallics* **2013**, *32*, 7249–7263.
- (43) Bose, R. N.; Fonkeng, B.; Barr-David, G.; Farrell, R. P.; Judd, R. J.; Lay, P. A.; Sangster, D. F. *J. Am. Chem. Soc.* **1996**, *118*, 7139–7144.
- (44) Niu, S. Q.; Hall, M. B. *Chem. Rev.* **2000**, *100*, 353–405.
- (45) Malakoff, D. *Science* **2014**, *344*, 1464–1467.
- (46) (a) Haibach, M. C.; Kundu, S.; Brookhart, M.; Goldman, A. S. *Acc. Chem. Res.* **2012**, *45*, 947–958. (b) Choi, J.; MacArthur, A. H. R.; Brookhart, M.; Goldman, A. S. *Chem. Rev.* **2011**, *111*, 1761–1779.
- (47) (a) Eisenstein, O.; Crabtree, R. H. *New J. Chem.* **2001**, *25*, 665–666. (b) Baudry, D.; Ephritikhine, M.; Felkin, H. *J. Chem. Soc., Chem. Commun.* **1982**, 606–607. (c) Baudry, D.; Ephritikhine, M.; Felkin, H. *J. Chem. Soc., Chem. Commun.* **1980**, 1243–1244. (d) Gupta, M.; Hagen, C.; Kaska, W. C.; Cramer, R. E.; Jensen, C. M. *J. Am. Chem. Soc.* **1997**, *119*, 840–841. (e) Belli, J.; Jensen, C. M. *Organometallics* **1996**, *15*, 1532–1534.
- (48) (a) Weckhuysen, B. M.; Schoonheydt, R. A. *Catal. Today* **1999**, *51*, 223–232. (b) Coperet, C. *Chem. Rev.* **2010**, *110*, 656–680. (c) Olsbye, U.; Virnovskaia, A.; Prytz, Ø.; Tinnemans, S.; Weckhuysen, B. *Catal. Lett.* **2005**, *103*, 143–148. (d) Weckhuysen, B. M.; Bensalem, A.; Schoonheydt, R. A. *J. Chem. Soc., Faraday Trans.* **1998**, *94*, 2011–2014. (e) Weckhuysen, B. M. *Phys. Chem. Chem. Phys.* **2003**, *5*, 4351–4360. (f) For related C–H bond activation on M–O sites, see: Hu, B.; Getsoian, A.; Schweitzer, N. M.; Das, U.; Kim, H. S.; Niklas, J.; Poluektov, O.; Curtiss, L. A.; Stair, P. C.; Miller, J. T.; Hock, A. S. *J. Catal.* **2014**, *322*, 24–37.
- (49) Siegbahn, P. E. M.; Svensson, M. *J. Am. Chem. Soc.* **1994**, *116*, 10124–10128.
- (50) Siegbahn, P. E. M. *J. Am. Chem. Soc.* **1993**, *115*, 5803–5812.
- (51) (a) Joubert, J.; Salameh, A.; Krakoviack, V.; Delbecq, F.; Sautet, P.; Copéret, C.; Basset, J. M. *J. Phys. Chem. B* **2006**, *110*, 23944–23950. (b) Wischert, R.; Copéret, C.; Delbecq, F.; Sautet, P. *Angew. Chem., Int. Ed.* **2011**, *50*, 3202–3205. (c) Wischert, R.; Laurent, P.; Coperet, C.; Delbecq, F.; Sautet, P. *J. Am. Chem. Soc.* **2012**, *134*, 14430–14449.
- (52) (a) Maron, L.; Perrin, L.; Eisenstein, O. *J. Chem. Soc., Dalton Trans.* **2002**, 534–539. (b) Coperet, C.; Grouiller, A.; Basset, J. M.; Chermette, H. *ChemPhysChem* **2003**, *4*, 608–611. (c) Werkema, E. L.; Maron, L.; Eisenstein, O.; Andersen, R. A. *J. Am. Chem. Soc.* **2007**, *129*, 6662–6662.
- (53) (a) Stephens, P. J.; Devlin, F. J.; Chabalowski, C. F.; Frisch, M. J. *J. Phys. Chem.* **1994**, *98*, 11623–11627. (b) Miehlisch, B.; Savin, A.; Stoll, H.; Preuss, H. *Chem. Phys. Lett.* **1989**, *157*, 200–206. (c) Lee, C. T.; Yang, W. T.; Parr, R. G. *Phys. Rev. B: Condens. Matter* **1988**, *37*,

- 785–789. (d) Becke, A. D. *J. Chem. Phys.* **1993**, *98*, 5648–5652.
- (e) Vosko, S. H.; Wilk, L.; Nusair, M. *Can. J. Phys.* **1980**, *58*, 1200–1211.
- (54) Frisch, M. J.; Trucks, G. W.; Schlegel, H. B.; Scuseria, G. E.; Robb, M. A.; Cheeseman, J. R.; Scalmani, G.; Barone, V.; Mennucci, B.; Petersson, G. A.; Nakatsuji, H.; Caricato, M.; Li, X.; Hratchian, H. P.; Izmaylov, A. F.; Bloino, J.; Zheng, G.; Sonnenberg, J. L.; Hada, M.; Ehara, M.; Toyota, K.; Fukuda, R.; Hasegawa, J.; Ishida, M.; Nakajima, T.; Honda, Y.; Kitao, O.; Nakai, H.; Vreven, T.; Montgomery, J. A., Jr.; Peralta, J. E.; Ogliaro, F.; Bearpark, M.; Heyd, J. J.; Brothers, E.; Kudin, K. N.; Staroverov, V. N.; Kobayashi, R.; Normand, J.; Raghavachari, K.; Rendell, A.; Burant, J. C.; Iyengar, S. S.; Tomasi, J.; Cossi, M.; Rega, N.; Millam, J. M.; Klene, M.; Knox, J. E.; Cross, J. B.; Bakken, V.; Adamo, C.; Jaramillo, J.; Gomperts, R.; Stratmann, R. E.; Yazyev, O.; Austin, A. J.; Cammi, R.; Pomelli, C.; Ochterski, J. W.; Martin, R. L.; Morokuma, K.; Zakrzewski, V. G.; Voth, G. A.; Salvador, P.; Dannenberg, J. J.; Dapprich, S.; Daniels, A. D.; Farkas, Ö.; Foresman, J. B.; Ortiz, J. V.; Cioslowski, J.; Fox, D. J. *Gaussian 09*, revision D.01; Gaussian, Inc.: Wallingford, CT, 2009.
- (55) (a) Hay, P. J.; Wadt, W. R. *J. Chem. Phys.* **1985**, *82*, 299–310. (b) Hay, P. J.; Wadt, W. R. *J. Chem. Phys.* **1985**, *82*, 270–283. (c) Wadt, W. R.; Hay, P. J. *J. Chem. Phys.* **1985**, *82*, 284–298.
- (56) (a) Krishnan, R.; Binkley, J. S.; Seeger, R.; Pople, J. A. *J. Chem. Phys.* **1980**, *72*, 650–654. (b) Mclean, A. D.; Chandler, G. S. *J. Chem. Phys.* **1980**, *72*, 5639–5648.
- (57) (a) Roy, L. E.; Hay, P. J.; Martin, R. L. *J. Chem. Theory Comput.* **2008**, *4*, 1029–1031. (b) Ehlers, A. W.; Bohme, M.; Dapprich, S.; Gobbi, A.; Hollwarth, A.; Jonas, V.; Kohler, K. F.; Stegmann, R.; Veldkamp, A.; Frenking, G. *Chem. Phys. Lett.* **1993**, *208*, 111–114.
- (58) (a) Frisch, M. J.; Pople, J. A.; Binkley, J. S. *J. Chem. Phys.* **1984**, *80*, 3265–3269. (b) Clark, T.; Chandrasekhar, J.; Spitznagel, G. W.; Schleyer, P. V. *J. Comput. Chem.* **1983**, *4*, 294–301.
- (59) Grimme, S.; Antony, J.; Ehrlich, S.; Krieg, H. *J. Chem. Phys.* **2010**, *132*, 154104–154119.
- (60) Grimme, S.; Ehrlich, S.; Goerigk, L. *J. Comput. Chem.* **2011**, *32*, 1456–1465.